Green Solid Electrolyte with Cofunctionalized Nanocellulose/Graphene Oxide Interpenetrating Network for Electrochemical Gas Sensors

*Jing Zhang, Gaopeng Jiang, Maciej Goledzinowski, Felix J. E. Comeau, Kecheng Li, Timothy Cumberland, Jared Lenos, Pan Xu, Matthew Li, Aiping Yu, and Zhongwei Chen**

A cofunctionalized cellulose/graphene oxide (GO) proton-conducting solid electrolyte with a 3D interpenetrating network structure is developed in an efficient and green strategy, and successfully applied in an electrochemical gas sensor for the detection of alcohol, namely an alcohol fuel-cell sensor. With grafted sulfonic acid groups onto the surface of cellulose nanofibers and GO nanosheets, the membrane is endowed with proton conductivity along both the through-plane and the in-plane ion-transport channels. The alcohol fuel-cell sensor equipped with cofunctionalized cellulose/GO membrane demonstrates great responses to ethanol vapor at different concentrations, showing excellent linearity and sensitivity, as well as low ethanol-detection limits approaching 25 ppm. This novel concept of developing a cofunctionalized cellulose/GO membrane opens a promising route for the application of ion-conducting solid electrolyte in electrochemical devices, particularly in electrochemical gas sensors.

1. Introduction

Gas sensors have seen a booming market owing to the ever-increasing demand of multitudinous gas detection and monitoring in industrial process, public and domestic air quality, food and drug safety, and automotive systems.[1,2] Based on different physical, chemical, and electronic mechanisms, gas-sensor devices have various types including semiconducting metal oxide sensor, electrochemical sensor, optical sensor, catalytic combustion sensor, etc.[3] For example, semiconducting metal oxide sensors widely exploit 2D metal oxide materials to detect target gas by physisorption and chemisorption processes originating from their enhanced surface to volume ratio and high-surface-area oxides. Moreover, some gasochromic oxides, such as MoO_3, WO_3, and Nb_2O_5, have sensitivity to exposed reducing gases by color changing.[4] Among all the sensors, electrochemical gas sensors, which operate by reacting with the gas of interest and outputting an electrical signal proportional to the gas concentration, has attracted much attention due to its selective, accurate, and linear response for target gas components in a complex environment.[5,6] Recently, in order to overcome the aqueous electrolyte leakage problems, electrochemical gas sensors are moving toward an all-solid-state package with the requirement of portability and safety.[2,7] Several conventional ceramic solid electrolytes have the capability to conduct ions at high temperature, and thus can be employed to construct all-solid-state gas sensors, such as yttria-stabilized-zirconia-based oxygen sensor and sodium-superionic-conductor-based chlorine gas sensor.[6,8] However, efficient solid ion-conducting electrolyte at room temperature is still a challenge for solid electrochemical gas sensor.[6]

Cellulose, one of the most sustainable and environmentally friendly materials on the planet, is currently widely utilized in electrochemical systems.[9] Owing to its specific linear chain molecular structure consisting of repeated glucose units with many exposed surface hydroxyl groups, cellulose is easily chemically modified to conduct protons or hydroxide ions at room temperature, and can be applied as an ion-conducting electrolyte.[10,11] Also, due to its hydrogen bonds and van der Walls forces between the hydroxyl groups on the surface of fibers, cellulose can be fabricated into a stable 3D fibrous membrane.[12] However, because of its fibrous network structure, cellulose membrane fails to block gases flowing through its inner porous channels, resulting in unsuccessful application as solid electrolyte in electrochemical gas sensors individually. Some specific 2D materials, such as molybdenum disulfide (MoS_2), graphene, graphene oxide (GO), have relatively strong absorption

J. Zhang, G. Jiang, T. Cumberland, J. Lenos, P. Xu, M. Li, Prof. A. Yu, Prof. Z. Chen
Department of Chemical Engineering
Waterloo Institute for Nanotechnology
Waterloo Institute of Sustainable Energy
University of Waterloo
200 University Ave. W, Waterloo, Ontario N2L 3G1, Canada
E-mail: zhwchen@uwaterloo.ca

Dr. M. Goledzinowski, F. J. E. Comeau
Alcohol Countermeasure Systems Corp
60 International Boulevard, Toronto, Ontario M9W 6J2, Canada

Prof. K. Li
Department of Chemical and Paper Engineering
Western Michigan University
1903 W Michigan Ave, Kalamazoo, MI 49008-5462, USA

The ORCID identification number(s) for the author(s) of this article can be found under https://doi.org/10.1002/smtd.201700237.

DOI: 10.1002/smtd.201700237

or barrier performance to gas molecules, owing to their basal surfaces and prismatic edges.[13,14] For example, MoS_2 shows a high affinity to selected model gas species because of the strong adsorption energy of gas molecules to the basal surface of 2D MoS_2.[13] Among all the 2D materials, GO, which has low permeability of most gases such as methanol, ethanol, methane, and carbon dioxide,[6,15] is expected to be utilized as an effective additive into cellulose-based solid electrolyte to tune its gas permeation. Moreover, due to the abundant oxygen-containing groups, GO can be covalently crosslinked with cellulose fibers and chemically modified with a host of functional groups,[16,17] making it an ideal candidate material in electrochemical gas-sensor applications.

Here, taking advantage of the unique properties of both cellulose and GO, a cofunctionalized cellulose-based membrane with GO modification was developed and applied as solid electrolyte in an electrochemical gas sensor for the detection of alcohol (ethanol). As shown in **Figure 1**a, the ethanol gas sensor is designed on the basis of direct ethanol fuel cell principle, namely alcohol fuel cell sensor (AFCS). When the ethanol molecules diffuse into the anode, the ethanol oxidation reaction is triggered, releasing protons and electrons. Protons

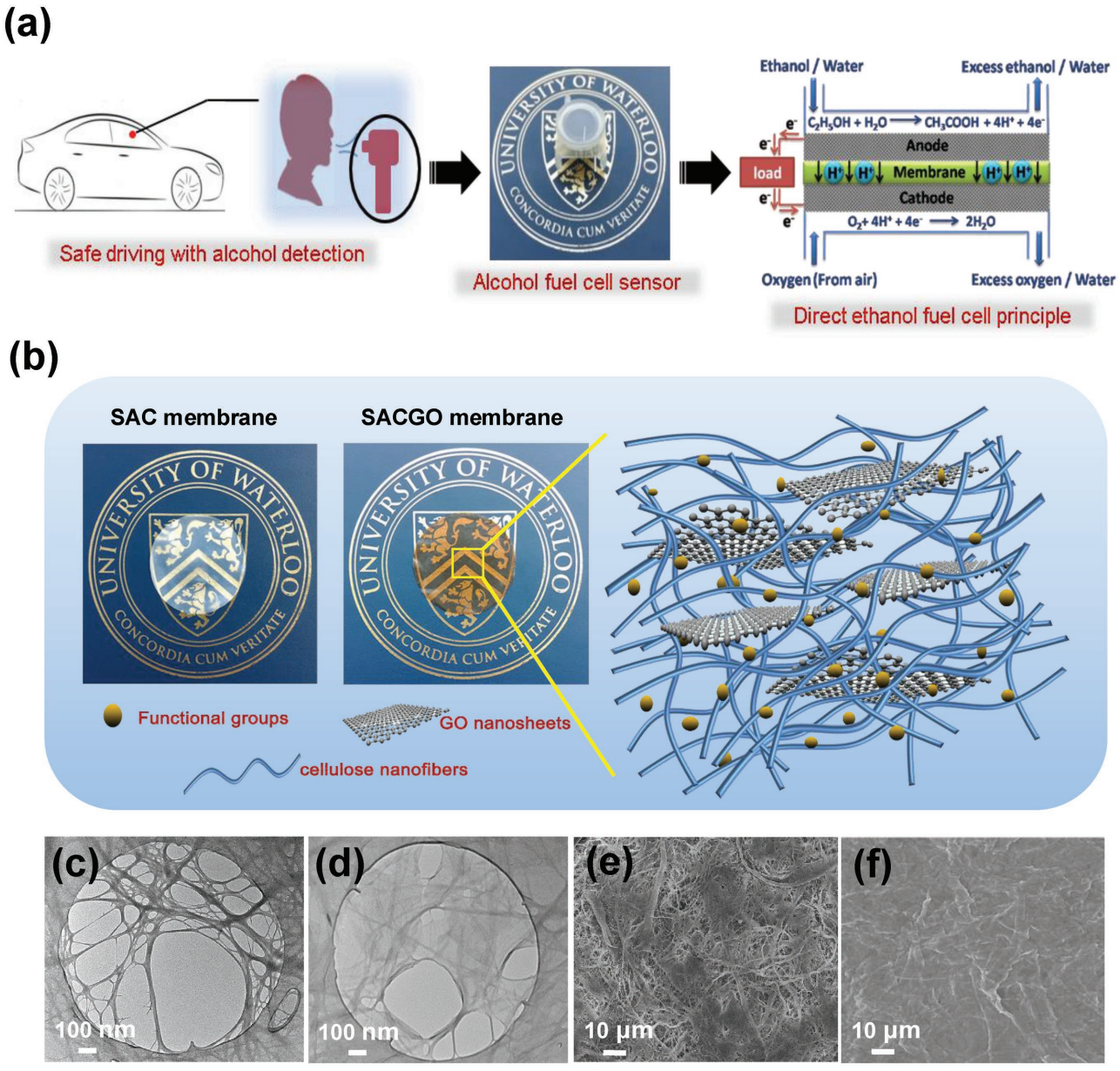

Figure 1. a) Schematic diagram of an AFCS and its electrochemical principle. b) Photographs of SAC and SACGO membranes, and schematic illustration of SACGO membrane's inner 3D interpenetrating structure. c) A TEM image of cellulose nanofibers. d) A TEM image of cellulose nanofibers wrapped and covered by GO nanosheets. e) A SEM image of SAC membrane with a fibrous network surface. f) A SEM image of SACGO membrane with a flat and dense surface (SACGO membrane here indicates the cellulose matrix mixing with 6% weight percentage of GO, i.e., 6-SACGO).

travel through the solid electrolyte and react with the oxygen from the air at the cathode, undergoing oxygen reduction reaction and generating water as the product. Transferred electrons from the anode to cathode are collected as the electrical signals that could provide information on the concentration of input ethanol vapor. A promising response to ethanol vapor was achieved for the AFCS made from cofunctionalized cellulose/GO membrane, showing excellent linearity as well as sensitive response to the alcohol detection with a low limit of 25 ppm. The appreciable characteristics demonstrate a new possibility for environmentally benign cellulose-based materials utilized as ion-conducting solid electrolyte in electrochemical systems, particularly in electrochemical gas sensor.

2. Results and Discussion

2.1. Material Synthesis and Structural Characterization

As shown in Figure S1 (Supporting Information), 3-mercaptopropyl trimethoxysilane (MPTMS) is selected as functional precursor to conduct the functionalization. First, trimethoxysilyl groups on MPTMS are hydrolyzed and self-condensed to form the corresponding silanol oligomer intermediates. After being absorbed onto the oxygen-containing groups through hydrogen bonding, these intermediates are covalently bonded to the surface of cellulose nanofibers and GO nanosheets through the removal of water molecules. Then, the mercapto groups on the tail end of MPTMS are oxidized to sulfonic acid (SA) groups, enduing both cellulose and GO the ability to conduct protons. Finally, the SA-functionalized mixture of cellulose nanofibers and GO nanosheets is vacuum filtered into membrane (Figure 1b). As shown in Figure 1b schematic illustration, the cellulose nanofibers are wrapped and covered by GO nanosheets, and reciprocally GO nanosheets are inserted into the network of cellulose nanofibers, resulting in a 3D interpenetrating network structure. The numerous cellulose nanofibers interlace into a stable network structure by hydrogen bonds and van der Waals force,[18] giving the membrane a tough and robust skeleton. Meanwhile, the GO nanosheets are inserted into and assembled with the whole cellulose fibrous skeleton, creating barrier layers to prevent ethanol gas penetration. The transmission electron microscopy (TEM) image (Figure 1c) shows an entangling and complex network-like structure of cellulose nanofibers. After the addition of GO, the cellulose nanofiber network is uniformly covered by the GO nanosheets (Figure 1d). The surface morphologies of membranes are further characterized by scanning electron microscopy (SEM). In the absence of GO, the SA-functionalized cellulose (SAC) membrane exhibits a fibrous and rough surface (Figure 1e), while the SA-cofunctionalized cellulose/GO (SACGO) membrane shows a dense and smooth surface (Figure 1f) due to the coverage of GO nanosheets within this cellulose-based system.

To confirm the successful sulfonic acid functionalization reaction, Fourier transform infrared (FTIR) spectra of non-functionalized cellulose/GO (CGO) membrane and SACGO membrane are compared in **Figure 2**a. In the spectrum of CGO membrane, the peak at 3344 cm^{-1} is assigned to vibration–stretching hydroxyl groups, while peak occurred at 2900 cm^{-1} is assigned to vibration–stretching of C—H.[19] Small peaks at 1300–1450 cm^{-1} region are corresponding to the HCH and OCH in-plane bending vibration, C—H in-plane bending, and CH_2 rocking vibration of cellulose.[16,20] The representative peaks located around 1037–1162 cm^{-1} are due to C—O stretching and C—O—C asymmetric vibration. The glucose ring stretching produces two peaks at 1112 and 898 cm^{-1}.[19,21] After functionalization, the FTIR spectrum of SACGO membrane reveals relatively weakened assigned peaks of O—H stretching, C—O—C vibration, and C—O stretching, which indicate the successful grafting reaction between the oxygen-containing groups on cellulose/GO and MPTMS. Alternatively, a new small peak at 809 cm^{-1} emerges in the spectrum, owing to the vibration of Si—O—C in the silane groups of the functional precursor MPTMS.[6,22]

The X-ray photoelectron spectroscopy (XPS) analysis of CGO and SACGO membrane is carried out to complement the FTIR results. The structural changes are analyzed by high-resolution spectra of C 1s, where five different peaks before functionalization are deconvoluted in Figure 2b, namely O—C=O (289.1 eV), O—C—O (287.9 eV), C—O—C (287.2 eV), C—O (286.5 eV), C—C/C—H (284.9 eV).[6,23] Similarly, after functionalization, the C 1s spectra of SACGO membrane also shows these five characteristic peaks (Figure 2c), but the peak intensity of C—O—C significantly decreases, which is in agreement with the results of FTIR, indicating the successful reaction between oxygen-containing groups of cellulose/GO and MPTMS. Meanwhile, a new peak at 285.6 eV assigned to C—S, C—O—Si of the grafted precursor MPTMS emerges,[24] indicating the presence of the SA functional groups on the surface of cellulose nanofibers and GO nanosheets, corroborating our previous FTIR results.

To further elucidate the existence and distribution of the grafted functional groups on cellulose and GO surface, a cross-sectional energy-dispersive X-ray spectroscopy (EDX) mapping of SACGO membrane is exhibited in Figure 2e–i. It can be found that elements Si and S (contained in the silane and sulfonic acid moieties of the grafted groups) with C and O are homogeneously distributed through the thickness of the membrane, indicating the successful functionalization in SACGO membrane. From the SEM cross-sectional view of SACGO membrane (Figure 2d), a 3D layered structure is observed through SACGO membrane. The typical structure of membrane has been proved to be effective to tune the ionic conductivities through the control of water uptake and ion transport channels.[10,11]

2.2. Proton Conductivity

In consideration of proton conductivity value (σ), it is important to note that, proton conductivity is commonly measured along the plane of the membrane, i.e., in-plane proton conductivity.[25,26] However, in practice, the proton conductivity perpendicular to the membrane, i.e., through-plane proton conductivity, is much more relevant for most applications.[27] Different membrane casting methods and membrane pretreatment procedures could lead to morphological anisotropy and hence result in anisotropic ionic conductivity.[25] Therefore, relying only on in-plane conductivity to estimate the ion transportation ability is inaccurate in case of membrane exhibiting morphological anisotropy.

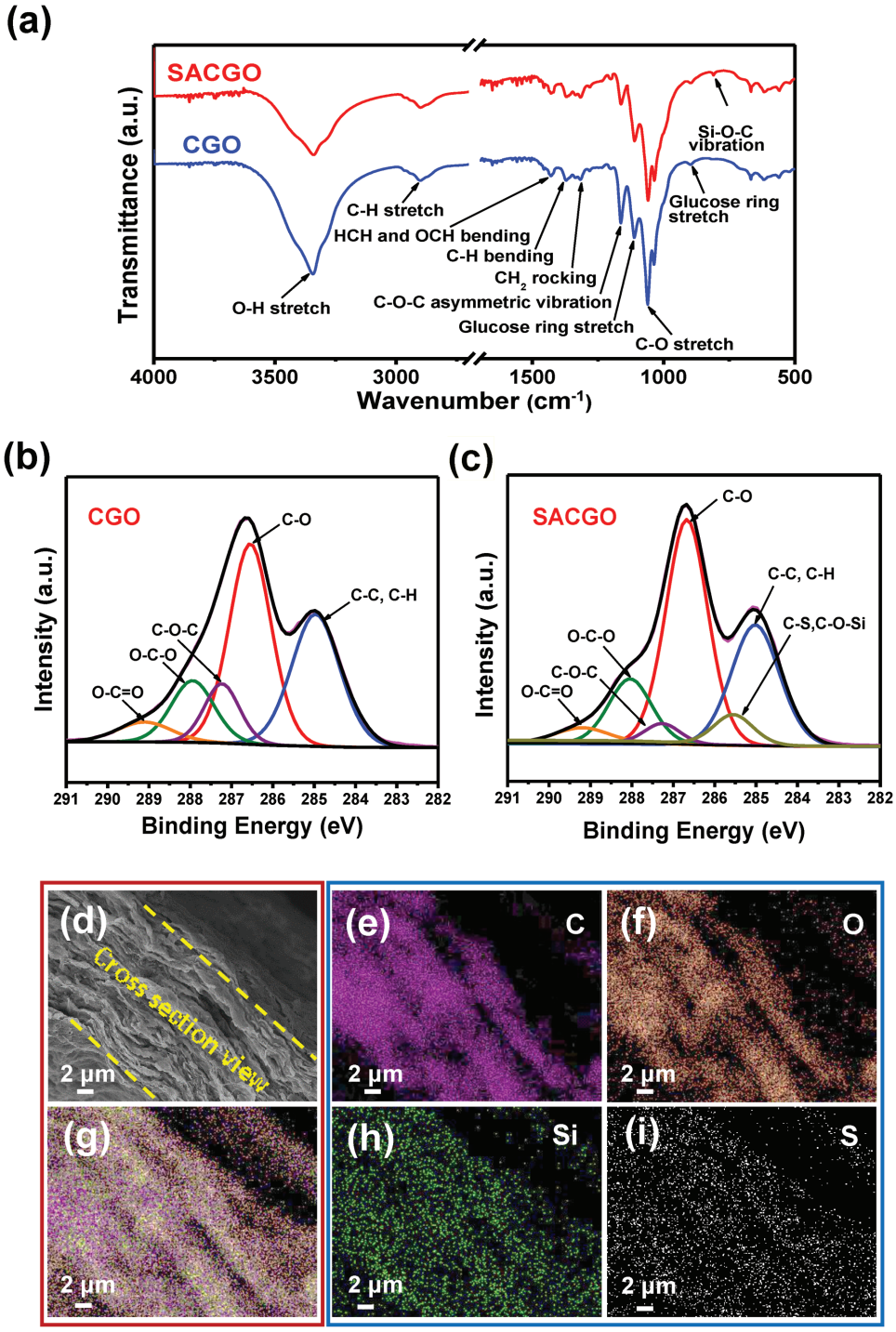

Figure 2. a) FTIR spectra. b,c) Deconvoluted XPS spectra in the C 1s region of CGO and SACGO membranes. d) Cross-sectional SEM image of SACGO membrane. e–i) EDX mapping images of the cross-section of SACGO membrane (SACGO membrane here indicates the cellulose matrix mixing with 6% weight percentage of GO, i.e., 6-SACGO).

In this work, in order to study the in-plane and through-plane proton conductivity for cellulose and GO composite system, the membranes were prepared by mixing 3%, 6%, and 10% weight percentage of GO into cellulose matrix, denoted as 3-SACGO, 6-SACGO, and 10-SACGO. As shown in **Figure 3**a, the in-plane conductivity (8.73 mS cm^{-1}) of SAC membrane is significantly improved compared to that of the nonfunctionalized pristine cellulose (PC) membrane (0.44 mS cm^{-1}, Figure S4, Supporting Information), indicating the successful graft of SA groups onto cellulose nanofibers. With further addition of GO into cellulose matrix, the in-plane conductivity gradually raises up to 26.86 mS cm^{-1} (10-SACGO membrane), which means that

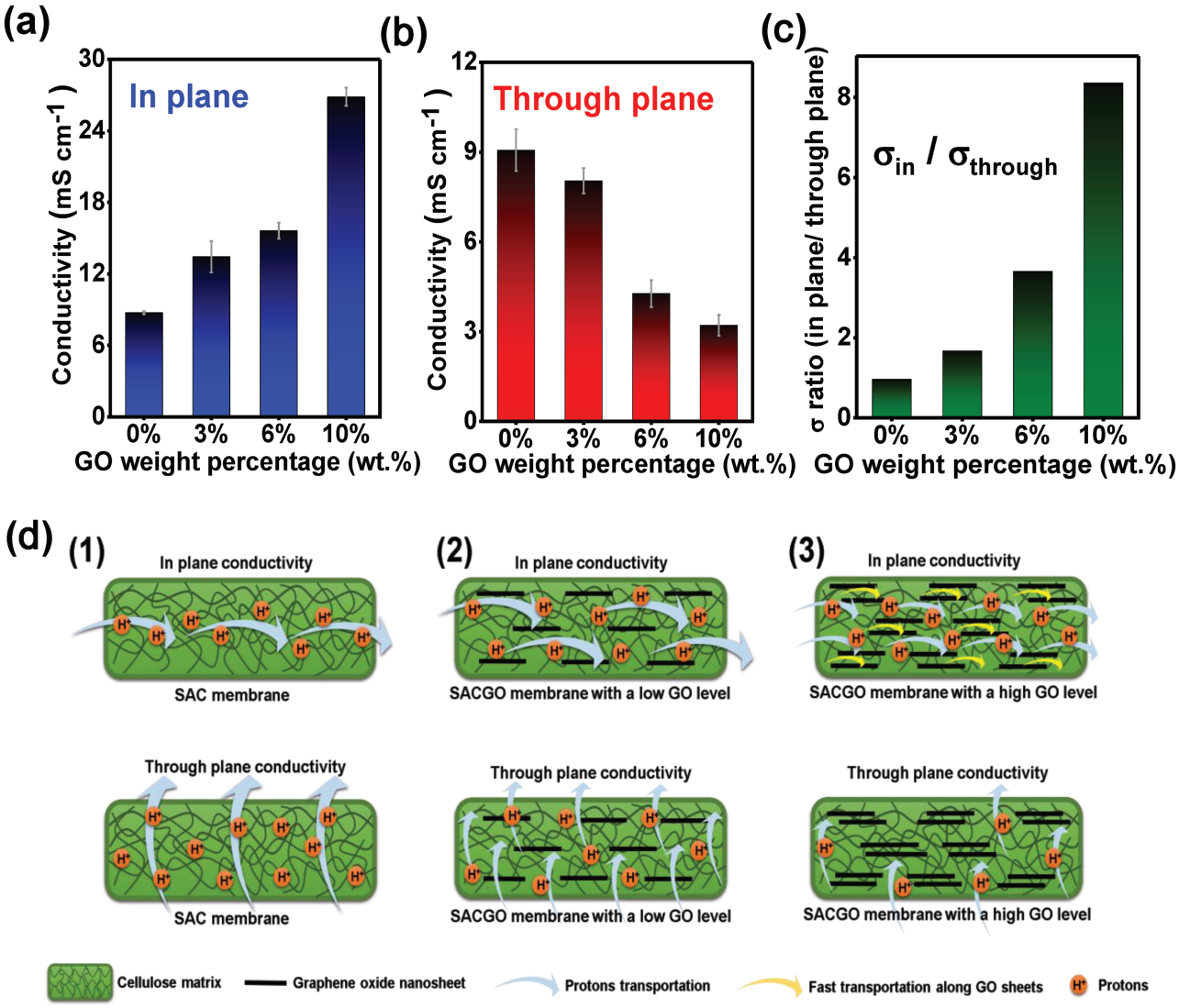

Figure 3. a,b) In-plane (a) and through-plane (b) proton conductivities of the SAC and SACGO membranes. c) Anisotropic conductivity values of SAC and SACGO membranes. d) A schematic illustration of ion transport mechanism with SAC and SACGO membranes with different GO additive levels.

the existence of SA-functionalized GO facilitates the migration of protons along the plane of the membrane. That is because GO exhibits effective ionic conductivity along the surface of 2D nanosheets. Meanwhile, the insertion of SA-functionalized GO into cellulose nanofiber network could form opened and layered ion-transport channels along the membrane inner structure.[28] Similarly, as shown in Figure 3b and Figure S4 (Supporting Information), the through-plane conductivity of SAC membrane is also remarkably higher than that of nonfunctionalized PC membrane (9.07 vs 0.59 mS cm^{-1}). However, with increasing GO weight percentage into cellulose matrix, the through-plane conductivity exhibits a gradual descending trend from 9.07 (SAC membrane) to 3.21 mS cm^{-1} (10-SACGO membrane). The decrease of through-plane conductivity is mainly due to the GO nanosheet self-assembly along the plane that blocks the ion transportation through the direction of the thickness.[29]

In order to further investigate the proton transportation, the anisotropy values of cellulose/GO membranes are calculated and exhibited in Figure 3c according to the ratio of in-plane to through-plane conductivities. The SAC membrane exhibits isotropic characteristic with anisotropy value of 0.96, indicating that the protons can almost be transported equally in both horizontal and vertical directions, and allowed to move freely in the membrane (Figure 3d(1)). However, after the addition of SA-functionalized GO, the in-plane conductivities of 3-SACGO and 6-SACGO membranes are obviously higher compared to those of through-plane counterpart with the anisotropy values of 1.67 and 3.66, respectively. This anisotropic ionic conductivity is mainly due to the insertion of SA-functionalized GO into the cellulose nanofiber network, which creates proton transportation channels along the plane of the membrane as well as the impermeable blocking layers that limit the protons to transport through the thickness of the membrane (Figure 3d(2)). Particularly, for 10-SACGO membrane, the in-plane conductivity exceeds its through-plane counterpart by eight times higher, in which the SA-functionalized GO layers stack within the

cellulose matrix causing a huge impediment for protons transporting across the membrane but fast proton transportation channels along the GO nanosheets (Figure 3d(3)). Therefore, the excess addition of GO into cellulose matrix (e.g., 10-SACGO membrane) is not suitable for practical applications because of the dramatic decrease of through-plane conductivity.

Water uptake of the membrane is a critical factor for proton conductivity. In the presence of water molecules, protons can be dissociated from the grafted SA groups and then hydrated into oxonium ions.[6] With the aid of oxonium ions, protons can be passed along the hydrogen bonds, or directly transport as a moving H_3O^+ "vehicle."[30] Accordingly, water molecule is indispensable during ion transportation, and high water uptake would be favorable for ionic conductivity. As shown in Figure S5 (Supporting Information), the water uptakes of the cellulose/GO membranes are around 90%, which is obviously higher than that of the commercial proton-conducting Nafion membrane (34.5%).[31] That is owing to the excellent hydrophilic nature of cellulose nanofibers and the fibrous and porous network of the membrane which play an important role in absorbing and retaining water within the internal structure.[11] In consequence, the high water uptakes of these cellulose/GO membranes assist protons in moving along and through the plane of membrane, resulting in promising ionic conductivity.

2.3. Sensor Performance

The practical performance of the cellulose/GO membrane as solid electrolyte for AFCS is demonstrated in a setup consisting of flow meter, water trap, alcohol simulator, sensor, data logger, and computer analyzer (Figure S7 and S8, Supporting Information). The core component of sensor is membrane electrode assembly (MEA), in which the membrane is sandwiched between two commercial gas diffusion electrodes (GDEs) loaded with Pt/C catalyst. In order to mimic the relative temperature and humidity of human breath, a constant of air is pumped through the alcohol simulator. Then, a certain concentration of ethanol vapor will be carried out with the air and enter into the sensor. In the sensor, the ethanol vapor is sampled, and the electrochemical reaction occurs. Next, the electrical signal is generated, collected, and finally analyzed in the terminal computer, outputting a typical response current curve characterized by four different parameters, namely response time, recovery time, peak height, and peak area (Figure S8, Supporting Information). In theory, peak area corresponds to the quantity of transferred electrons which is in proportion to the amount of reacted ethanol molecules. Accordingly, the ethanol concentration shows a linear relationship with the peak area, and can be used for calculated by Equation (1):

$$c = \frac{A_{\text{peak}}}{nFV} \tag{1}$$

where c is the ethanol concentration in the vapor, A_{peak} is the peak area, n is the number of transferred electrons in the electrochemical reaction, F is the Faraday constant, and V is the fixed volume of ethanol vapor sampled into the sensor.

In **Figure 4**b, the performance of sensors made from nonfunctionalized PC, SAC, and SACGO membranes are tested in ethanol standard solution equivalent to blood alcohol concentration (BAC) of 50 mg dL^{-1}. BAC is defined as the number of milligrams of alcohol per 100 mL of blood. Evidently, the SACGO membrane has the highest peak area and peak height among these three membranes, indicating its potential application in AFCS. Compared to the PC, the SAC membrane with functionalized sulfonic acid groups can easily conduct protons in its inner structure, resulting in higher sensitivity to ethanol. However, as shown in Figure 4a, the residual ethanol vapor after electrochemical reaction may pass through the SAC membrane from the anode to cathode because of its porous network structure, and finally causing the gas permeate problem. Therefore, with the addition of SA-functionalized GO which is less permeable to most gases, the SACGO membrane exhibits better sensor performance due to its resistance to ethanol vapor mass transfer. After 30 d, the SACGO-membrane-based sensor shows an almost unchanged response curve from its initial test, demonstrating its excellent stability (Figure 4c). Additionally, in Figure 4d, the sensor prepared from SACGO membrane can effectively response to an ethanol standard solution equivalent to BAC of as low as 10 mg dL^{-1}, corresponding to the detected limit of 25 ppm ethanol in human breath. The peak area of the SACGO-based sensor is also calculated as a function of different concentrations of ethanol standard solution, which shows great linearity (Figure 4e). Selectivity is another critical issue for gas sensors. In order to further investigate selectivity performance, the SACGO-based sensor was tested in response to water, ethanol, and acetone vapor in the equal liquid concentration. As shown in Figure S9 (Supporting Information), the SACGO-based sensor demonstrates excellent selectivity of ethanol over water and acetone. Virtually, no response curves of water and acetone were observed, but obvious ethanol response was detected in the same concentration.

3. Conclusion

In conclusion, for the first time, a cofunctionalized cellulose-based proton-conducting membrane with GO modification is fabricated and successfully applied as solid electrolyte in an electrochemical gas sensor for the detection of alcohol. Both promising in-plane and through-plane conductivities, as well as high water retention within the 3D interpenetrating network structure are achieved for SACGO membrane as an effective proton-conducting solid electrolyte, indicating successful graft of sulfonic acid groups onto cellulose and GO surface. An AFCS setup is created and further demonstrated the promising electrochemical performance of cellulose/GO membrane, where stable and liner response curves to ethanol vapor are obtained with the ethanol-detection limit of as low as 25 ppm. Therefore, this novel concept of cellulose/GO system in this work will open a possible route for the development of ion-conducting solid electrolyte in electrochemical device, particularly in electrochemical gas sensors.

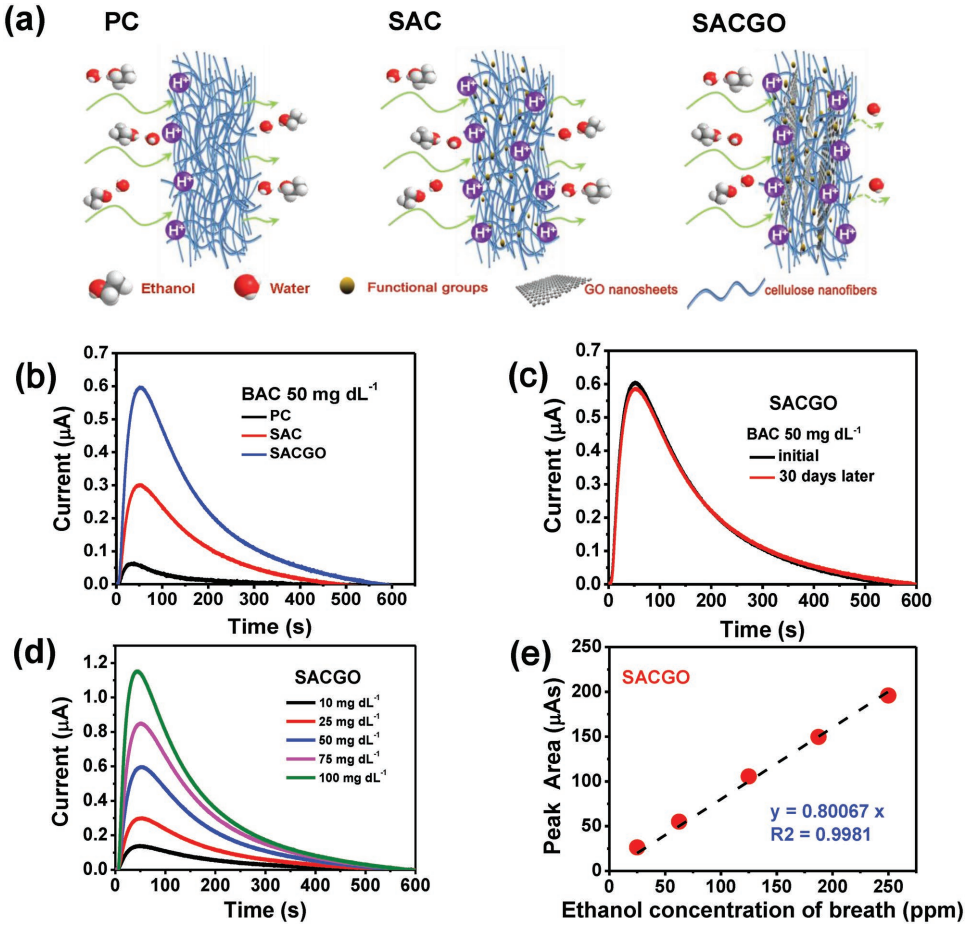

Figure 4. a) The schematic of protons and ethanol vapor transportation in cellulose/GO membrane. b) Response curves of sensor employing PC, SAC, and SACGO membranes. c) The initial and 30 d after response curves of SACGO-based sensor to the ethanol vapor from standard solution equivalent to BAC of 50 mg dL^{-1}. d) Response curves of SACGO-based sensor to the ethanol vapor from different standard solutions. e) The peak areas obtained from response curves versus ethanol concentration in the vapor (SACGO membrane here indicates the cellulose matrix mixing with 6% weight percentage of GO, i.e., 6-SACGO).

4. Experimental Section

Synthesis of GO: The synthesis of GO was in accordance with the improved Hummers' method.[32] First, 98% H_2SO_4 (360 mL) and 85% H_3PO_4 (40 mL) were mixed carefully in a round-bottom flask under an ice bath condition. Graphite powder (2 g) was added into the concentrated mixed acid and mechanically stirred for 1 h. Then, the strong oxidizing agent, $KMnO_4$ (18 g) was added slowly into the mixture, and the oxidation reaction was kept at 50 °C for 16 h. The oxidation reaction was terminated by cooling down the mixture. Distilled deionized (DDI) water (400 mL) and H_2O_2 (20 mL) were added dropwise into the mixture and stirred for 30 min. Afterward, the mixture was centrifuged and washed with DDI water, 5% HCl, and ethanol, respectively. Finally, the GO nanosheets were obtained by freeze-drying of GO suspension.

Preparation of Cellulose Nanofibers: The cellulose nanofibers were prepared from northern bleached softwood kraft pulp (New Brunswick, Canada) through prerefining, enzymatic processing, and nanorefining. First, the original pulp was disintegrated by using the Noram PFI mill (Quebec, Canada) with up to 30 000 rpm. Then, an enzyme treatment was proceeded with mixture of two enzymes (i.e., mannanase and xylanase) from Novozymes (Franklinton, USA) to gain a uniform pulp suspension. Finally, the enzyme treated pulp suspension was thoroughly washed with DDI water to remove any residues, and refined by PFI mill again with 30 000 rpm to produce cellulose nanofibers.

Fabrication of Functionalized Cellulose/GO Membrane: In order to obtain proton conductive cellulose/GO membrane, MPTMS was applied as precursor to functionalize cellulose nanofibers and GO nanosheets with sulfonic acid groups. First, cellulose was mixed with GO in ethanol by magnetic stirring for 2 h to obtain a uniform cellulose/GO suspension. The amount of GO in mixture varied 0%, 3%, 6%, and 10% with respect to the cellulose mass. Then, MPTMS was added dropwise into the cellulose/GO mixture with mass ration of 20:1 (MPTMS:mixture), and maintained at ambient temperature for 48 h. After washing with ethanol and DDI water to remove any unreacted trace of MPTMS, 30% H_2O_2 was added into the mixture and maintained at ambient temperature for 24 h. Afterward, the resulting solution was centrifuged and washed with DDI water to obtain the sulfonic acid-functionalized cellulose/GO. The resulting proton conductivity cellulose/GO membrane was fabricated by vacuum filtration and then dried at 60 °C under vacuum for 2 h.

Characterization and Electrochemical Measurement: The morphologies of cellulose nanofibers, GO nanosheets, and GO membranes were imaged by SEM (LEO 1530) and TEM (Bruker AXS D8 Advance). The chemistry and crystal structure of cellulose nanofibers, GO nanosheets, and GO membranes were analyzed by FTIR (Avatar 320), XPS (Thermo Scientific Al K_α X-ray source), and tension testing machine (ADMET 7603-5 kN). A mixed Gaussian–Lorentzian function was used while analyzing XPS peaks with a corrected Shirley background. The conductivities of membrane performed via electrochemical impedance spectroscopy (Princeton

Versastat MC potentiostat) were in frequency ranging from 100 kHz to 1 Hz with perturbation voltage amplitude of 100 mV.

Electrochemical-Gas-Sensor Evaluation: The electrochemical gas-sensor performance was evaluated by application of MEA with a series of cellulose/GO membranes. The MEA was fabricated by sandwiching the as-prepared membranes with commercial GDE (Fuel Cells Etc.). The commercial GDEs were coated with 60% Pt/C catalyst at a Pt loading of 0.5 mg cm^{-2} for both anode and cathode. Then, the MEA was punched into desired size and assembled into sensor housing with two Pt wires as current collectors. Before testing, the sensor housing with MEA assembled was stabled in the humidity chamber (BTL-433) with 25 °C and room humidity (RH) 60% for 72 h to equilibrate the components with the desired condition. The resulting sensor housing was then inserted into the testing device to evaluate the performance. Each sample was repeated five times and the average of each parameter was taken into account.

Supporting Information

Supporting Information is available from the Wiley Online Library or from the author.

Acknowledgements

The authors thank the support of the Alcohol Countermeasure Systems (International) Inc. This work was financially supported by the Natural Sciences and Engineering Research Council of Canada (NSERC), and the Ontario Centers of Excellence (OCE). All the financial supports are gratefully acknowledged.

Conflict of Interest

The authors declare no conflict of interest.

Keywords

cellulose, electrochemical gas sensors, graphene oxide, proton conductivity, solid electrolytes

Received: July 5, 2017
Published online: September 25, 2017

[1] Z. Q. Zheng, J. D. Yao, B. Wang, G. W. Yang, *Sci. Rep.* **2015**, *5*, 11070.
[2] J. Zhang, X. Liu, G. Neri, N. Pinna, *Adv. Mater.* **2016**, *28*, 795.
[3] a) C. Hagleitner, A. Hierlemann, D. Lange, A. Kummer, N. Kerness, O. Brand, H. Baltes, *Nature* **2001**, *414*, 293; b) A. Modi, N. Koratkar, E. Lass, B. Wei, P. M. Ajayan, *Nature* **2003**, *424*, 171.
[4] K. Kalantar-zadeh, J. Z. Ou, T. Daeneke, A. Mitchell, T. Sasaki, M. S. Fuhrer, *Appl. Mater. Today* **2016**, *5*, 73.
[5] a) C. Park, J. Fergus, N. Miura, J. Park, A. Choi, *Ionics* **2009**, *15*, 261; b) J. R. Stetter, W. R. Penrose, S. Yao, *J. Electrochem. Soc.* **2003**, *150*, S11.
[6] G. Jiang, M. Goledzinowski, F. J. Comeau, H. Zarrin, G. Lui, J. Lenos, A. Veileux, G. Liu, J. Zhang, S. Hemmati, *Adv. Funct. Mater.* **2016**, *26*, 1729.
[7] W. Zeng, L. Shu, Q. Li, S. Chen, F. Wang, X. M. Tao, *Adv. Mater.* **2014**, *26*, 5310.
[8] a) S. Yao, Y. Shimizu, N. Miura, N. Yamazoe, *Chem. Lett.* **1990**, *19*, 2033; b) H. Aono, Y. Sadaoka, *J. Electrochem. Soc.* **2000**, *147*, 4363.
[9] a) L. Hu, Y. Cui, *Energy Environ. Sci.* **2012**, *5*, 6423; b) L. Hu, M. Pasta, F. L. Mantia, L. Cui, S. Jeong, H. D. Deshazer, J. W. Choi, S. M. Han, Y. Cui, *Nano Lett.* **2010**, *10*, 708; c) H. Zhu, Z. Jia, Y. Chen, N. Weadock, J. Wan, O. Vaaland, X. Han, T. Li, L. Hu, *Nano Lett.* **2013**, *13*, 3093; d) L. Hu, N. Liu, M. Eskilsson, G. Zheng, J. McDonough, L. Wågberg, Y. Cui, *Nano Energy* **2013**, *2*, 138.
[10] J. Zhang, J. Fu, X. Song, G. Jiang, H. Zarrin, P. Xu, K. Li, A. Yu, Z. Chen, *Adv. Energy Mater.* **2016**, *6*, 1600476.
[11] J. Fu, J. Zhang, X. Song, H. Zarrin, X. Tian, J. Qiao, L. Rasen, K. Li, Z. Chen, *Energy Environ. Sci.* **2016**, *9*, 663.
[12] L. Hu, H. Wu, F. L. Mantia, Y. Yang, Y. Cui, *ACS Nano* **2010**, *4*, 5843.
[13] K. J. Berean, J. Z. Ou, T. Daeneke, B. J. Carey, E. P. Nguyen, Y. Wang, S. P. Russo, R. B. Kaner, K. Kalantar-Zadeh, *Small* **2015**, *11*, 5035.
[14] K. J. Berean, J. Z. Ou, M. Nour, M. R. Field, M. M. Y. A. Alsaif, Y. Wang, R. Ramanathan, V. Bansal, S. Kentish, C. M. Doherty, A. J. Hill, C. McSweeney, R. B. Kaner, K. Kalantar-zadeh, *J. Phys. Chem. C* **2015**, *119*, 13700.
[15] a) R. Kumar, M. Mamlouk, K. Scott, *Int. J. Electrochem.* **2011**, *2011*, 1; b) R. R. Nair, H. A. Wu, P. N. Jayaram, I. V. Grigorieva, A. K. Geim, *Science* **2012**, *335*, 442; c) R. K. Joshi, P. Carbone, F. C. Wang, V. G. Kravets, Y. Su, I. V. Grigorieva, H. A. Wu, A. K. Geim, R. R. Nair, *Science* **2014**, *343*, 752.
[16] a) L. L. Zhang, X. Zhao, M. D. Stoller, Y. Zhu, H. Ji, S. Murali, Y. Wu, S. Perales, B. Clevenger, R. S. Ruoff, *Nano Lett.* **2012**, *12*, 1806; b) D. A. Dikin, S. Stankovich, E. J. Zimney, R. D. Piner, G. H. Dommett, G. Evmenenko, S. T. Nguyen, R. S. Ruoff, *Nature* **2007**, *448*, 457.
[17] Y. Li, H. Zhu, S. Zhu, J. Wan, Z. Liu, O. Vaaland, S. Lacey, Z. Fang, H. Dai, T. Li, *NPG Asia Mater.* **2015**, *7*, e150.
[18] a) W. Bao, Z. Fang, J. Wan, J. Dai, H. Zhu, X. Han, X. Yang, C. Preston, L. Hu, *ACS Nano* **2014**, *8*, 10606; b) J. L. Morgan, J. Strumillo, J. Zimmer, *Nature* **2013**, *493*, 181.
[19] J. Zhang, L. Yue, P. Hu, Z. Liu, B. Qin, B. Zhang, Q. Wang, G. Ding, C. Zhang, X. Zhou, J. Yao, G. Cui, L. Chen, *Sci. Rep.* **2014**, *4*, 6272.
[20] a) S. Y. Oh, D. I. Yoo, Y. Shin, G. Seo, *Carbohydr. Res.* **2005**, *340*, 417; b) S. K. Mahadeva, K. Walus, B. Stoeber, *ACS Appl. Mater. Interfaces* **2014**, *6*, 7547.
[21] K. K. Sadasivuni, A. Kafy, L. Zhai, H. U. Ko, S. Mun, J. Kim, *Small* **2015**, *11*, 994.
[22] J.-L. Huang, C.-J. Li, D. G. Gray, *RSC Adv.* **2014**, *4*, 6965.
[23] a) Y. Chen, X. Zhang, D. Zhang, P. Yu, Y. Ma, *Carbon* **2011**, *49*, 573; b) S. Yokota, T. Kitaoka, J. Sugiyama, H. Wariishi, *Adv. Mater.* **2007**, *19*, 3368.
[24] a) H. Hamze, M. Jimenez, D. Deresmes, A. Beaurain, N. Nuns, M. Traisnel, *Appl. Surf. Sci.* **2014**, *315*, 531; b) M. Y. Bashouti, R. T. Tung, H. Haick, *Small* **2009**, *5*, 2761.
[25] T. Soboleva, Z. Xie, Z. Shi, E. Tsang, T. Navessin, S. Holdcroft, *J. Electroanal. Chem.* **2008**, *622*, 145.
[26] A. A. Argun, J. N. Ashcraft, P. T. Hammond, *Adv. Mater.* **2008**, *20*, 1539.
[27] J. Li, J. K. Park, R. B. Moore, L. A. Madsen, *Nat. Mater.* **2011**, *10*, 507.
[28] M. R. Karim, K. Hatakeyama, T. Matsui, H. Takehira, T. Taniguchi, M. Koinuma, Y. Matsumoto, T. Akutagawa, T. Nakamura, S. Noro, T. Yamada, H. Kitagawa, S. Hayami, *J. Am. Chem. Soc.* **2013**, *135*, 8097.
[29] K. Hatakeyama, M. R. Karim, C. Ogata, H. Tateishi, A. Funatsu, T. Taniguchi, M. Koinuma, S. Hayami, Y. Matsumoto, *Angew. Chem., Int. Ed.* **2014**, *53*, 6997.
[30] a) K.-D. Kreuer, A. Rabenau, W. Weppner, *Angew. Chem., Int. Ed. Engl.* **1982**, *21*, 208; b) T. J. F. Day, U. W. Schmitt, G. A. Voth, *J. Am. Chem. Soc.* **2000**, *122*, 12027; c) D. Marx, M. E. Tuckerman, J. Hutter, M. Parrinello, *Nature* **1999**, *397*, 601.
[31] a) S. K. Dishari, M. A. Hickner, *ACS Macro Lett.* **2012**, *1*, 291; b) Q. Li, *Solid State Ionics* **2004**, *168*, 177.
[32] D. C. Marcano, D. V. Kosynkin, J. M. Berlin, A. Sinitskii, Z. Sun, A. Slesarev, L. B. Alemany, W. Lu, J. M. Tour, *ACS Nano* **2010**, *4*, 4806.